AFCRL 62-244

GRD Research Notes
No. 76

BIOASTRONAUTICAL MEASUREMENTS OF IONIZING RADIATIONS IN SPACE: NUCLEAR EMULSION MONITORING REPORT

Herman Yagoda

February 1962

Project 8600
Task 86003

Ionospheric Physics Laboratory
GEOPHYSICS RESEARCH DIRECTORATE
AIR FORCE CAMBRIDGE RESEARCH LABORATORIES
OFFICE OF AEROSPACE RESEARCH
UNITED STATES AIR FORCE
Bedford, Massachusetts

Abstract

During the summer of 1960, a series of four instrumented balloons were launched from Bemidji, Minnesota to secure cosmic ray data at high elevations and to study the effects of the radiations on biological systems. It was hoped that one of the flights might be coincident with a solar flare which would give rise to a large increase in radiation dosage resulting from an influx of solar protons which at times penetrate the atmosphere in appreciable abundance at balloon elevations. Each of the flights carried small units of nuclear emulsion to provide standardization data for other electronic instrumentation and to serve as directional monitors for heavy primary radiation penetrating the brains of the animals. Measurements were made of star production frequencies, proton enders, and heavy primary thindown hits. As a measure of solar proton enhancement, counts were made of the frequency of proton track enders in the emulsion. The ender production was essentially constant on all four flights and varied between 498 and 604 tracks cc^{-1} hr^{-1}, in agreement with earlier measurements in Minnesota, indicating the absence of any flare phenomena. It is suggested that the ratio of proton enders to stars may prove a useful parameter for indicating exposure to solar protons at balloon elevations, and small doses of trapped particles in animals flown in space probes and satellites which approach or graze the lower Van Allen belt.

Acknowledgements

The assembly of the emulsion blocks and monitors and associated field work was performed by Robert Filz. The photographic processing of the exposed emulsions was carried out by Katsura Fukui. The reading of the plates was made with the patient assistance of Ernie Holeman and Albert Davis. The assistance rendered by these staff members of Emmanuel College is gratefully acknowledged.

Contents

Illustrations

Tables

BIOASTRONAUTICAL MEASUREMENTS OF IONIZING RADIATIONS IN SPACE: NUCLEAR EMULSION MONITORING REPORT

Introduction

Studies by the University of Minnesota cosmic ray workers (Winkler[9, 10] and Ney[3, 4]) have demonstrated the occurrence of large increases in the intensity of the cosmic radiation owing to the intermittent arrival of beams of low energy protons from the sun. At balloon elevations, the normal galactic cosmic ray beam produces ionization corresponding to a dose rate of about 0.0004 r/hr. However, on 1 April 1959, the dose rate increased to 0.053 r/hr and on 15 July 1959, a reading of 0.140 r/hr was obtained. Since the low energy solar protons responsible for the augmented ionization are rapidly stopped in the upper layer of the atmosphere, much larger increments can be anticipated for free space conditions. During large solar flares, dose rates as high as 30,000 r/hr have been extrapolated for free space condition from Pioneer V radiation measurements.

These unpredictable large increases in the environmental radiation field are of concern in manned flight near and above the top of the atmosphere. In January of 1960, Brig. Gen. Don Flickinger held a conference to discuss the nature of this new radiation hazard and to study the possibility of launching ionization monitors above the atmosphere during a major solar flare. With the time and facilities available, it was concluded that a series of large balloons which could achieve elevations exceeding 130,000 ft with payloads of several hundred pounds would be best suited for the task. The field operation was placed in charged of Major Russell E. Linkous of Kirkland Air Force Base. As shown in Table I, four Air Force Laboratories participated in the flight of diverse electronic and transistor counting equipment in an effort to study their performance prior to installation in deep space probes. Later in the program, the NASA Langley Research Center and the Armed Forces Institute of Pathology also took advantage of the launching facilities to expose mice to the high altitude radiations, the animals being monitored by the

Emulsion Cosmic Ray Group at AFCRL (See Section 1).

Table I. Nature of Payloads Exposed on July-August 1960 Bemidji Balloons

Organization	Payload (lbs)	Description
School of Aviation Medicine San Antonio, Texas	73	Black mice, Algae, Neurospora, seeds, etc.
Air Force Special Weapons Center, Albuquerque, N. M.	6.5	Ion chamber for dose rate measurements having range of 0.2 to 200 r/hr.
Holloman Air Force Base Aeromedical Laboratory Holloman, N. M.	67 190 5	Lockheed Counters Heavy Primary Counters Emulsions
Air Force Cambridge Research Laboratories, Bedford, Mass.	11	Emulsion Blocks
NASA-AFIP	19	Animal Sphere

The balloons of 6,000,000 and 9,000,000 cu ft capacity were launched by Raven Industries Inc., who were also responsible for the recovery of the payloads and the measurement of the time-altitude profiles of the vehicles. In order to minimize the deflecting effect on low energy charged particles by the earth's magnetic field, a far north point (within the confines of the USA) was called for. The launch site of Bemidji, Minnesota (geographic latitude 47.5°N, longitude 94.5°W, $\lambda = 58°$N) was selected. The flight trajectories are shown in Figs. 1 and 2, and details of the cosmic ray exposures are summarized in Table II.

On each of the four flights, AFCRL had a block of emulsions assembled from 1500-micron-thick G5 pellicles. The block was located high on the loadline to minimize shadow effects by the other massive equipment mounted below it. Each flight also carried three specially prepared glass plates coated with 600-micron-thick layers of G5 emulsion on both sides. The plates served to monitor heavy primary hits in the animals aboard the NASA-AFIP capsule. The emulsion blocks are described in Table III, and the preparation of the animal monitor plates are described in Section 1. Control plates of identical manufacture as those flown accompanied each parcel of emulsion to and

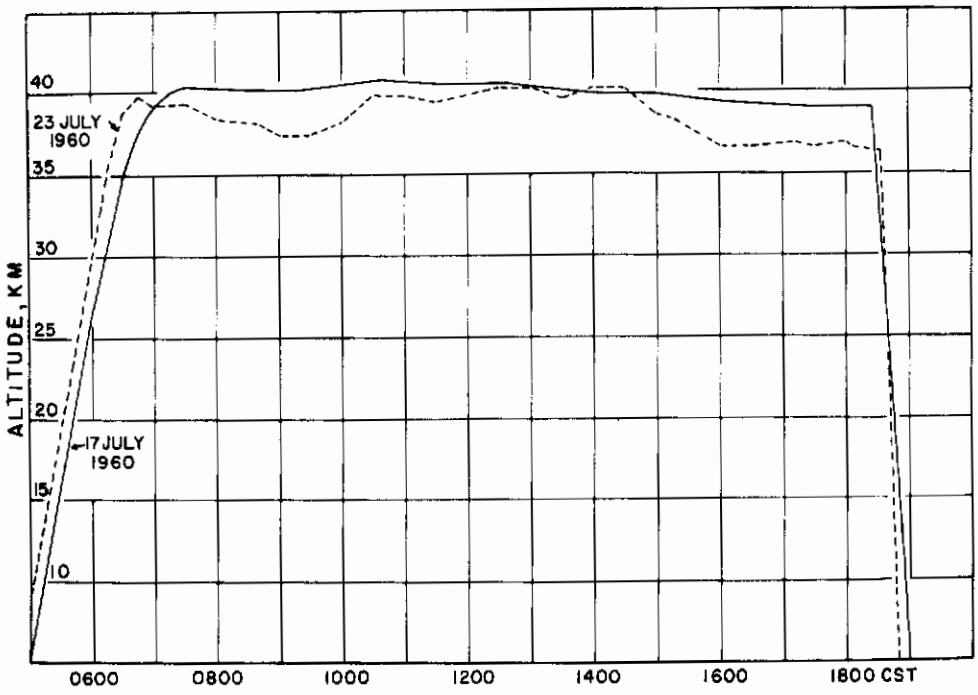

Figure 1. Flight trajectories of the 6 million cu ft balloons

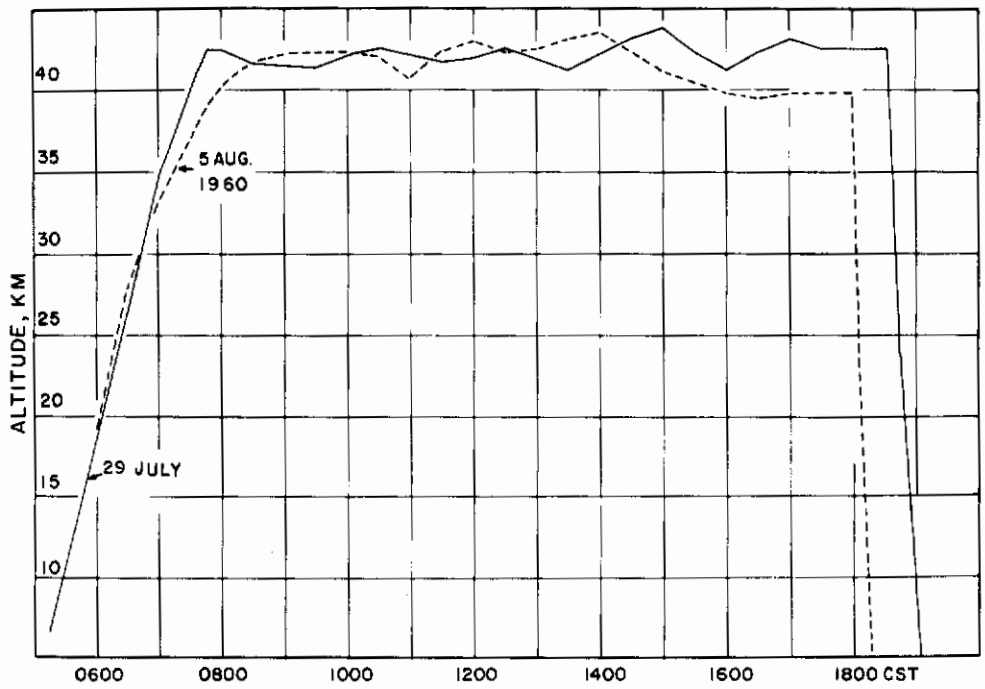

Figure 2. Flight trajectories of the 9 million cu ft balloons

Table II. Characteristics of Flight Trajectories

Launching Date	17 July 60	23 July 60	29 July 60	5 Aug 60
AFCRL No.	JKL	GHI	DEF	ABC
Balloon Volume	6,000,000	6,000,000	9,000,000	9,000,000
Total Payload, lb	584	588	469	604
Time of Launch, CST	0455	0434	0454	0456
Termination, CST	1826	1834	1834	1800
Impact, CST	1854	1905	1910	1912
Impact, Lat.	47° 8' N	48° 8' N	47° 14' N	48° 05' N
Long	107° 6' W	107° 40' W	107° 12' W	114° 23' W
Total Flight Time	14.0 hrs	14.52 hrs	14.27 hrs	14.27 hrs
Effective Time (hr) for:				
Star Production	11.58	12.25	10.93	10.13
Ender Production	13.48	13.52	13.18	12.46
H.P. Thindowns*	13.25	13.38	12.94	12.31
Max. Alt., km	40.8	40.2	43.8	43.6
Avg. Plateau Alt.	40.0	38.6	42.1	41.5
Avg. Plateau Air Mass	3.10	3.74	2.33	2.53
Zurich Sunspot No.	131	127	94	25

*Based on time spent at altitudes above 60,000 ft.

from the launching area. These plates served as a correction for background stars and proton ender populations.

With the exception of the 17 July flight, all the preparations were recovered in excellent condition. On the first flight the main balloon load was recovered, but the external parcel of emulsions was torn off and could not be located in the vicinity of the impact point. The present report is based largely on readings of the animal monitor plates, which proved particularly useful for the measurement of volume frequency phenomena since the thickness of the individual emulsion layers could be measured with a high degree of accuracy. From the construction of the animal capsule, we estimate that the monitor plates were exposed beneath 1.05 g cm^{-2} of condensed matter. While this is about five times greater than the 0.17 to 0.20 g cm^{-2} present on the external blocks, comparative measurements made on the flight of 29 July give, within the limits of statistical fluctuations, identical values of star production and heavy primary thindown terminations.

Table III. Characteristics of External Emulsion Blocks

Flight Date	17 July 60	23 July 60	29 July 60	5 Aug 60
Plateau Atmo. Depth, g cm^{-2}	3.10	3.75	2.34	2.52
Condensed Matter, g cm^{-2}	0.174	0.20	0.17	0.20
Total Vertical Absorber	3.27	3.95	2.51	2.72
Distance above NASA Capsule	30 ± 5 ft	Same	Same	Same
Vertical Face Dimensions	4 x 4 in	4 x 4	6 x 6	4 x 4
Wt. of Emulsion Block, g	3851	1315	1579	2121

1. Preparation of Animal Monitor Plates

In the absence of distortion due to photographic processing, the direction of an ionizing particle can be deduced from the track produced in a nuclear emulsion. From the direction cosines of the recorded line segment, the path can be extrapolated into matter below the plate, thus offering an opportunity to correlate damage to tissue, as discerned by histological staining techniques, with the passage of an individual densely-ionizing particle. If a single coating of emulsion is employed as the vectorial detector, some distortion is always present because the upper surface is free to swell and shift, whereas the lower surface bonded to the glass cannot do so. Also, as a result of the fixation process, the dry gelatin shrinks along the z-axis perpendicular to the xy-plane of the emulsion, so that its thickness is roughly one-half the original emulsion thickness. The original dip angle of the track can be reconstructed by application of a shrinkage factor correction $f_z = T/t$, where T is the original emulsion thickness and t is the final thickness of the residual gelatin. The original coating thickness, T, is usually known only approximately from the manufacturer's nominal rating. In a batch of plates coated 600 microns thick, individual members may vary by ± 15 microns from the mean. The gelatin thickness, t, is strongly dependent on glycerine pickup and relative humidity at the time of measurement. Because of these uncertainties, the recorded track is not a precise measure of the exact particle trajectory.

The line of flight of a nuclear particle can be determined with greater accuracy by using a doubly-coated plate which records two sections of the trajectory. As shown in Fig. 3a, a ray crossing this monitor provides two points (A and B) at the glass-emulsion interfaces that can be considered fixed and independent of changes in thickness due to photographic processing. The line AB in the final gelatin (Fig. 3b) thus defines the direction of the particle, since the thickness of the intermediary glass, AC = G, is not subject to appreciable change and can be measured accurately by means of the microscope fine adjustment movement. By orienting the plate so that the track is parallel to a precision screw microscope movement, the horizontal projection,

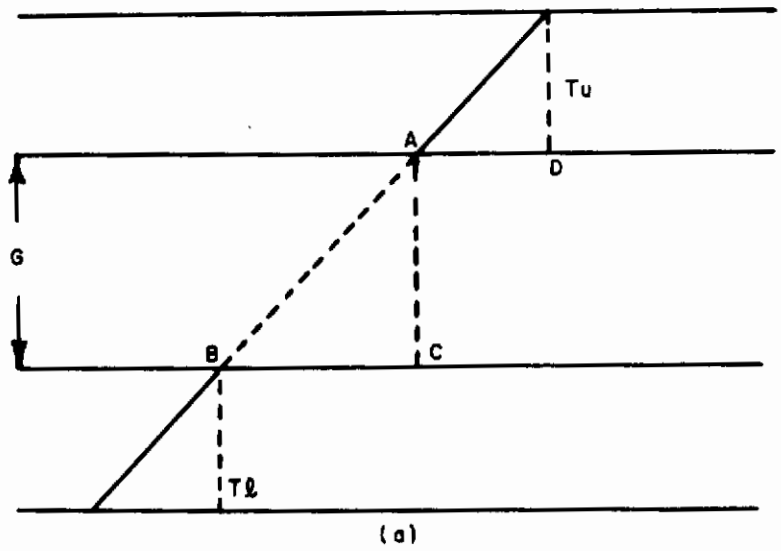

(a) original emulsion thickness

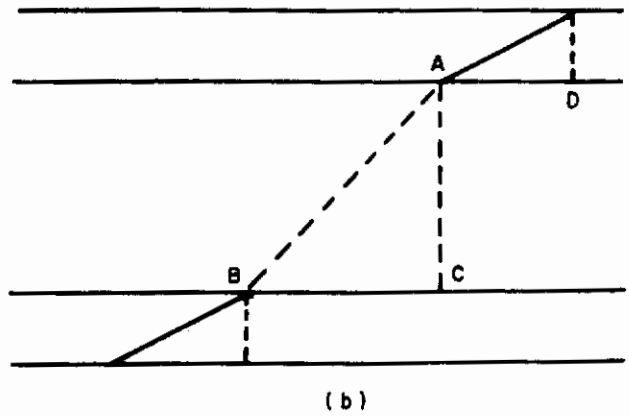

(b) after photographic processing

Figure 3. Cross-section of dual plate monitor

BC = d, can be measured with an accuracy of ± 2 microns. The true dip angle of the track is thus tan $\beta = G/d$.

The dual emulsion monitoring technique was first employed in conjunction with a series of animal flights conducted by the Aeromedical Laboratory of Holloman Air Force Base during the summer of 1958. In this early attempt at tracing heavy primaries through the brains of monkeys, the monitor was prepared as follows:[11]

An Ilford G5 plate, coated 600 microns thick on 1 mm thick glass, was supported emulsion face down on a sheet of absorbent paper. The glass surface was cleaned by scraping with a razor blade and degreasing with carbon tetrachloride. A G5 pellicle, somewhat larger than the plate, was moistened with distilled water containing a few drops of wetting agent, and the shiny side of the pellicle was pressed down against the clean glass with the aid of a rubber roller. The sandwich was covered with a sheet of polyethylene and pressed down with a 1/2 inch brass plate for 1 or 2 hours. After this setting process, the overlapping emulsion was trimmed away from the edges, and the plates were permitted to dry overnight at a relative humidity of 60 percent.

In an effort to expose the animals at elevations of about 140,000 ft, very thin polyethylene balloon envelopes were used. These envelopes tore during ascent, so that a heavy primary exposure could not be obtained. Development of the monitors revealed that the glued-on emulsion layer was subject to bubbling during processing, with serious distortion within these lifted areas. On the basis of this experience, the following alternate procedure was employed in the present investigation:

The glass sides of two Ilford G5 plates were cleaned and the 600-micron-thick emulsion layers were exposed at high humidity to remove bowing as a result of stresses in the dry emulsion. The glass backings were then bonded together by means of a 3 percent gelatin solution at 30°C. For the 6 x 4 inch plates, 50 drops of gelatin cement were applied to the center of one glass. The second plate was lowered onto the first and the excess solution wiped off. The unit was then clamped between paper-covered wooden blocks until the gelatin

was set. After overnight equilibration at 50 percent relative humidity, the plates were wrapped in black paper and rendered moisture-proof by means of parafilm sheeting and black polyethylene rubberized tapes. All the overlapping wrapping bonds were made on the upper face of the monitor to maintain the lower surface as flat and thin as feasible. The total bottom face wrappings in contact with the lucite animal cage averaged 0.35 ± .05 mm in thickness.

The back-to-back bonding of the glass plates has proven satisfactory, since the gelatin cement holds firm during the photographic processing and no blistering of the commercially prepared emulsion layers occurs. The separation between the emulsion layers is of the order of 2 mm; this places a constraint on depth measurements with conventional microscope objectives. The Koristka 30X oil immersion objective has a working distance of 3 mm and a numerical aperture of 1.05, and is thus adequate for accurate depth measurements. The fine adjustment of the Koristka R 4 microscope has a total range of 4 mm, thus, both sensitive layers can be viewed and measured despite the overall thickness of about 3.5 mm for the composite unit. By selecting an immersion oil with a refractive index close to that of glass, comparative tests show that the optical thickness measurements are indistinguishable from the mechanical thickness measured by contact dial gauges. Measurements of the glass thickness over the length of the plate show that the bonding procedure yields a uniform slab, with deviations of ± 0.3 percent from the mean thickness.

2. Extrapolation of Heavy Primary Trajectory into Brain Tissue (Prepared by Robert Filz, AFCRL)

As described in Section 1, the developed monitor plates provide for each track two points (A and B) whose position is unaffected by the photographic processing. A line drawn through AB provides a vector for estimating the points of intersection of the heavy primary in the tissue. One duplex plate was mounted in a fixed position above each cage, and served as a monitor for four animals. The head of each animal was maintained in a fixed position, so that the center point of each head was known relative to the fixed edges of the plate. The geometric relationship between the head of the animal and the

monitor is shown in Fig. 4. Thus, a coordinate net system could be set up on the microscope stage, using the x-axis as the base line for the back of the brain and the y-axis passing through the brain center as indicated in Fig. 5. These axes correspond to an identical set of axes drawn on the animal housing plate holder.

The general geometric approach is illustrated in Fig. 6 which shows two rays passing through the monitor plate and traversing an idealized slab confining the brain. For a perpendicular incident ray (α) the situation is simple, since the points of brain penetration (p-q) are a direct vertical extension of points a and b as seen through the microscope. For inclined tracks, such as β, the position of points P and Q can be computed from a knowledge of the distance S = W + C (see Fig. 4), the measured glass thickness, G, and the thickness of the bottom emulsion layer, T_1. The position of point P is also dependent on the thickness of the skin and bone above the brain, a quantity not defined in this experiment. Therefore, two planes were selected, separated by a distance M = 1 cm, which would be more than adequate to confine the greatest depth of brain plus its skull and skin covering. The x and y coordinates of points P and Q are thus:

$$x_P = x_A + (x_B - x_A) \frac{(S + T_1 + G)}{G}$$

$$y_P = y_A = (y_B - y_A) \frac{(S + T_1 + G)}{G}$$

$$x_Q = x_A + (x_B - x_A) \frac{(S + T_1 + G + M)}{G}$$

$$y_Q = y_A + (y_B - y_A) \frac{(S + T_1 + G + M)}{G}$$

Points P and Q can now be plotted on a graph (Fig. 5) containing an outline of the horizontal projection of the brain on the same scale. If P-Q falls within the outline, a heavy primary traversal through the brain tissue can be assumed, subject to the following limitations:

(1) The rectangular slab of constant thickness, M, is a very crude

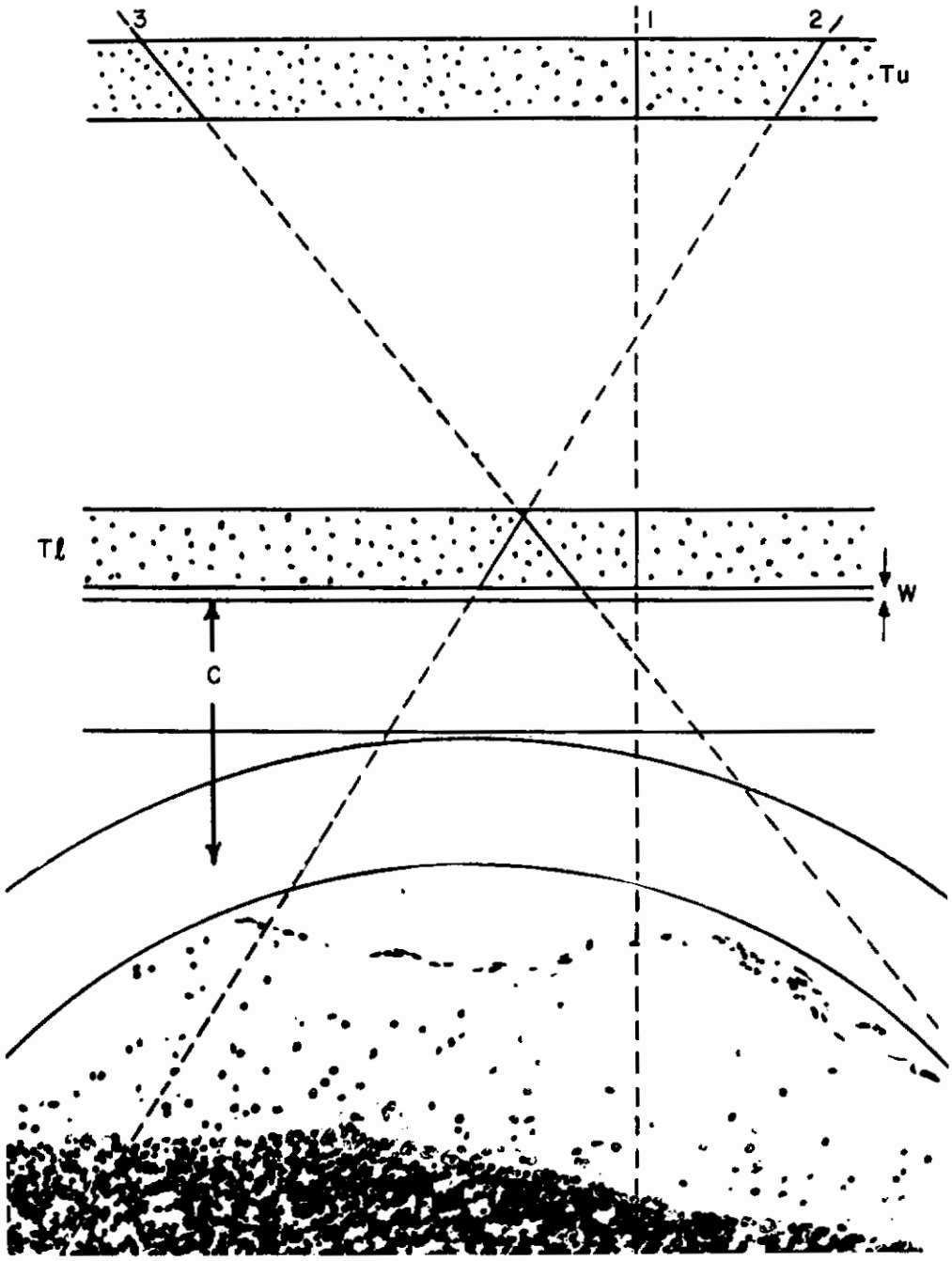

Figure 4. Geometry of track monitor relative to animal head.

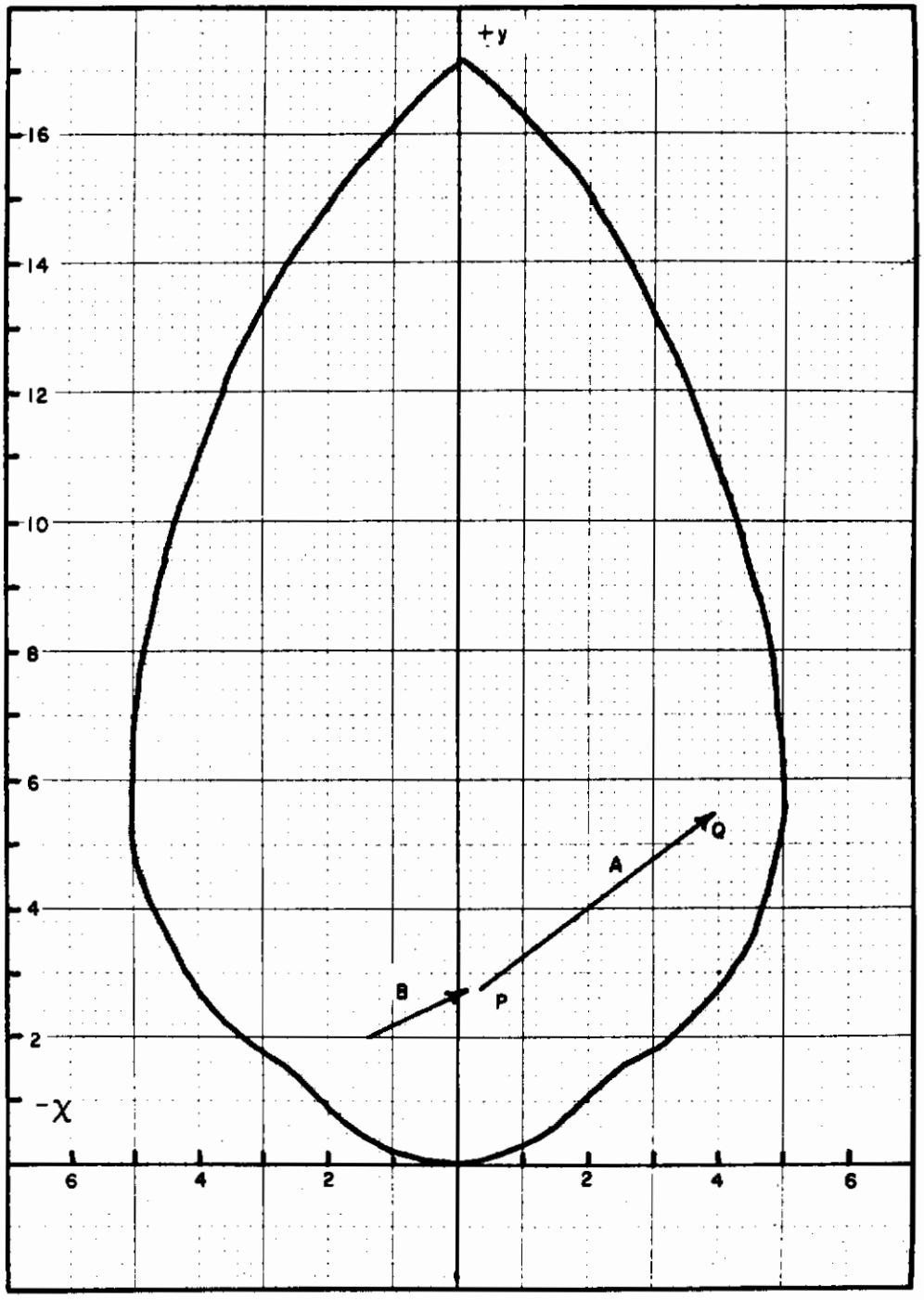

Figure 5. Coordinate system of tracks relative to xy-plane of mouse brain. Tracks A and B represent the extrapolated trajectories of particles A and B shown in Figure 7.

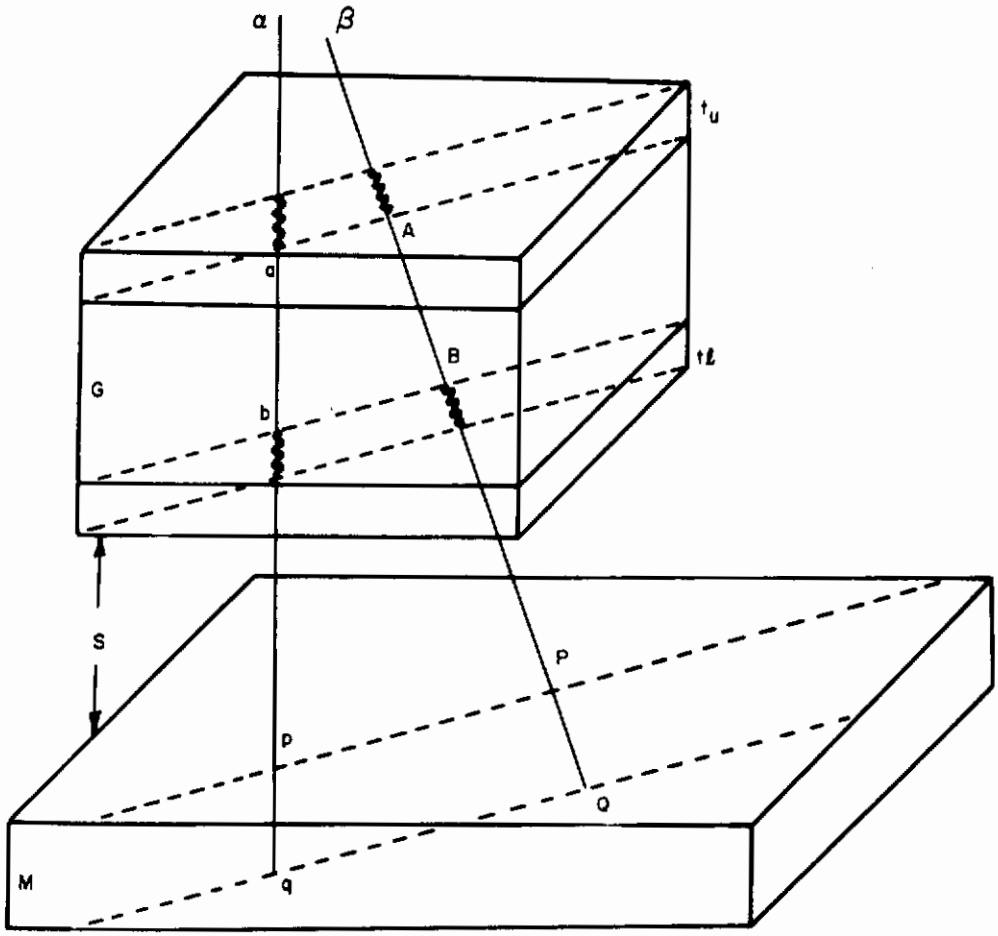

Figure 6. Trajectory extrapolation from tracks in monitor plate into an idealized slab confining the brain.

approximation of the true shape of the brain. This organ has a maximum thickness near the center line and thins out near the edges, roughly approximating an almond shape. Thus, certain rays may pass above the brain even though point P falls within the horizontal projection.

(2) Owing to the accumulated reading errors in measuring points A and B, coupled with uncertainties in S and in the location of the plane containing the brain entry point, the extrapolation of long flat tracks has not been attempted. Our vectorial scanning has been confined to tracks that make angles with the vertical $\theta \leq 30^\circ$ in the vicinity of the animal head. The brain could be traversed, however, by particles that entered at large angles to the vertical at points far removed from the head.

(3) Heavy primary nuclei have large collision cross-sections and may be destroyed while traversing region S. Likewise, slow heavy primaries can stop by ionization in this region before reaching the brain. For the very heavy nuclei of charges $Z \geq 20$, it is estimated that the collision loss is less than 2 percent for 0 to 30° angles, in an absorber 0.2 g cm^{-2} thick. At larger angles to the vertical, the attenuation increases and is 5 percent for a 75° ray. In the absence of an energy spectrum distribution for very slow heavy primaries, it is difficult to estimate the fraction of the beam which will stop by ionization in the intervening absorber of thickness S. However, it is often possible to detect these particles by the different appearance of the track in the upper and lower layers of the monitor. If the lower emulsion layer shows the beginning of a taper, there is a good probability that the particle will not reach the brain even though properly directed. In exposures at balloon elevations the tracks will enter only from the upper hemisphere, particles directed from beneath being absorbed in the atmosphere. It should be noted that the track image in the microscope usually is an inversion of the true geometric direction. The nature of the change, caused by mirrors and prisms in the optical system, is best determined by focusing on a miniature arrow with the same microscope. Stereo-binocular microscopes give a three-dimensional image which correlates with the geometric vector. The heavy tracks under considerations are readily resolved with these low power instruments.

This microscopic surveying technique revealed that, on the average, the animal brains received three hits by heavy primaries which entered the detector at zenith angles $\theta \leq 30°$. From geometric considerations an additional five particles, which entered at angles between 30° and 75°, traversed the brain. Measurements were made only on very dense tracks, such as those reproduced in the photomicrograph of Fig. 7, at A and B. It is difficult to estimate the charge of these steeply oriented tracks because of the (1) large density of the delta rays; (2) their coalescence owing to emulsion shrinkage; and (3) because the velocity of the particles is unknown. However, if we assume that the bulk of the particles were non-relativistic, a rough delta ray count by the method described by Yagoda[13] yields 15 as a lower unit of the charge on track A. In the same field of view, track B which appears more opaque than A because of its greater steepness, is probably of the same order of charge ($Z \geq 16$). About one third of the steep tracks which entered the brain were of this charge category. The rest of the analyzed tracks had had charges of 12 ± 3.

The location of tracks whose extrapolated line of flight (PQ) appeared to pass through the brain was studied in our laboratories by members of the Armed Forces Institute of Pathology. From their knowledge of the shape of the brain profile, they were able to eliminate some rays which either grazed or failed to penetrate brain tissue. In view of the difficulties of securing trajectories of flat tracks, it was agreed that these would be further studied only if the correlation between biological damage and the steep track passages appeared to warrant the effort.

3. Star Production Rates and Star Prong Spectra

The nuclear evaporation rate is a measure of both the primary and secondary nucleonic cosmic ray components incident on the emulsion detector. Following conventional methods, a tally was made of stars constituted of $N_h \geq 3$ black or gray tracks. In the case of three-pronged stars the event was accepted provided one of the tracks had a range ≥ 60 microns. Short recoil tracks were counted provided their range exceeded 5 microns. Stars produced by the capture of slow negative pi mesons were excluded. The star

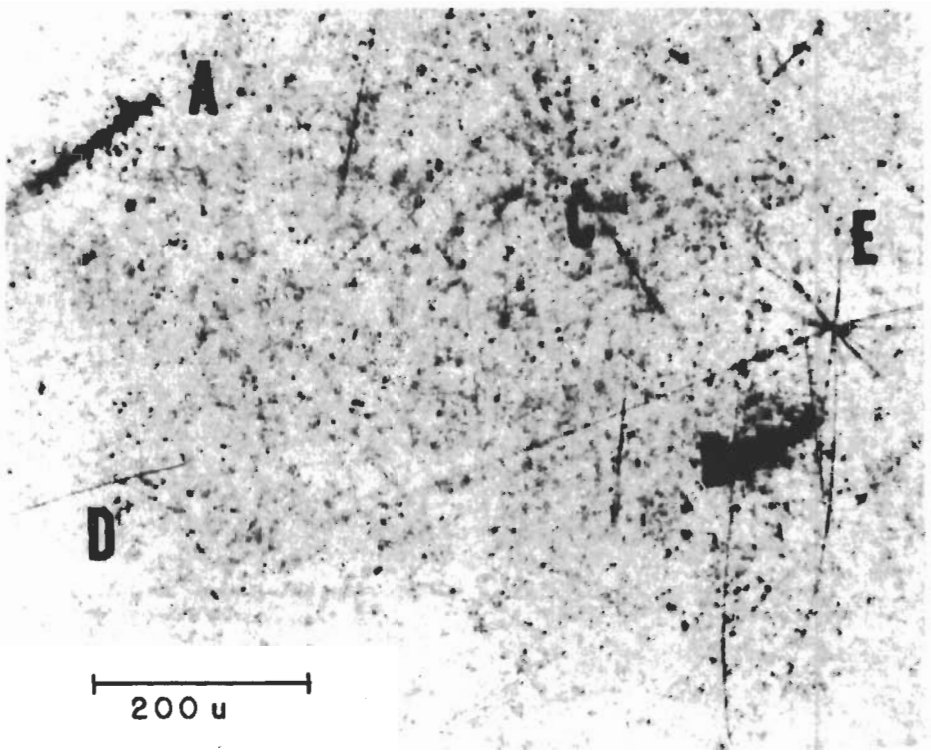

Figure 7. Photomicrograph of upper layer of monitor plate K-c showing relative appearance of steep heavy primary tracks produced by particles of about charge 16 or greater.

A. particle entering at 24° with vertical
B. particle entering at 10° with vertical
C. light nucleus of roughly charge 6 entering at 30° with vertical
D. flat track of stopping alpha particle
E. nuclear evaporation event (star)

counts were made with 40X oil immersion objectives, sampling swaths defined by two parallel cross hairs in the oculars. In the case of the animal monitor plates, the thickness of the emulsion layer was estimated from T = G 1/d, where 1 is the length of the horizontal projection of a track crossing the monitor (as shown in Fig. 3).

The results of this study are summarized in Table IV. Two corrections (A and B) had to be applied, in order to obtain a true star production rate for the period when the balloon floated at plateau. Because of the continuous sensitivity of the emulsion, stars are recorded between manufacture and development, especially when the plates are transported by airplane. This correction, A, is made from a star count on a plate of identical history, which is sent to the launching grounds but is not flown on the balloons. The average star population in the control plates was 289 ± 35 cc^{-1}. The total star population also has to be corrected for star production during the ascending phase of the balloon and while the payload is being brought down by parachute (B). Ideally, corrections A and B are best made simultaneously, by flying a monitor plate to the plateau altitude and allowing it to drop when the balloon reaches its ceiling.

Table IV. Star Production in Bemidji Flights

Flight Date	17 July 60	23 July 60	29 July 60	5 Aug 60
Avg. Plateau Altitude	40.0 Km	38.6 Km	42.1 Km	41.5 Km
Total Star Count	346	446	406	457
Volume, cc	0.2712	0.3722	0.3092	0.3370
Total Stars, cc^{-1}	1276	1198	1313	1356
Correction A, cc^{-1}	289	289	289	289
Correction B, cc^{-1}	132	102	167	176
Plateau Stars, cc^{-1}	855	807	857	891
Stars, cc^{-1} day^{-1}	1772 ± 163	1581 ± 128	1882 ± 166	2111 ± 175

Since an exposure of this character was not available, we have estimated correction B by assuming that the star production rate diminishes exponentially with atmospheric depth x. We used a function P (stars) = 1900 exp (-x/140), which is in good agreement with experimental data in the lower atmosphere as indicated in Fig. 8. The data near sea level and from mountain tops are based on observations by Teucher[6] and Yagoda[12].

As shown in Table IV, the star production rate for the four balloon flights varied between the narrow limits of 1580 to 2110 cc^{-1} day^{-1}, in general agreement with the range of values for stratospheric balloon flights at essentially the same geomagnetic latitude. The first two flights, which had a lower ceiling altitude than the latter ones, show smaller star production rates, indicating that at the small atmospheric depths of this experiment the star production rate still appears to be increasing slowly with increase in altitude.

The star size distribution based on 1647 events, located systematically in plates from the four balloon flights, is exhibited by curve A of Fig. 9. A similar study of the integral star size distribution for events recorded in the control plates is shown in curve B. Both spectra show a discontinuity at about $N_h = 7$ or 8, as noted by other investigators.[1, 5] Birnbaum[1] attributes the difference in slope of the exponential functions for small and large stars ($N_h \geq 8$) to the chemical composition of the emulsion which is composed of two groups of nuclei. The target atoms of the gelatin of nuclear charge 6, 7, and 8 are basically capable of yielding only stars of $N_h \leq 6$ prongs, whereas the larger stars of $N_h \geq 8$ prongs must originate from the evaporation of more massive nuclei such as silver or bromine. However, if the raw data in curve A is corrected for stars accumulated at lower elevations, by means of loci B, then the discontinuity in the star spectrum recorded during the high altitude flight C becomes markedly reduced. Small stars will also record during the ascending phase of the balloon. Likewise, when the payload is large, low energy secondaries are also produced during the period of stratospheric flight and will tend to augment the relative percentage of small stars recorded in the emulsion. Taking these factors into consideration, our observations suggest that in the high altitude exposure of an emul-

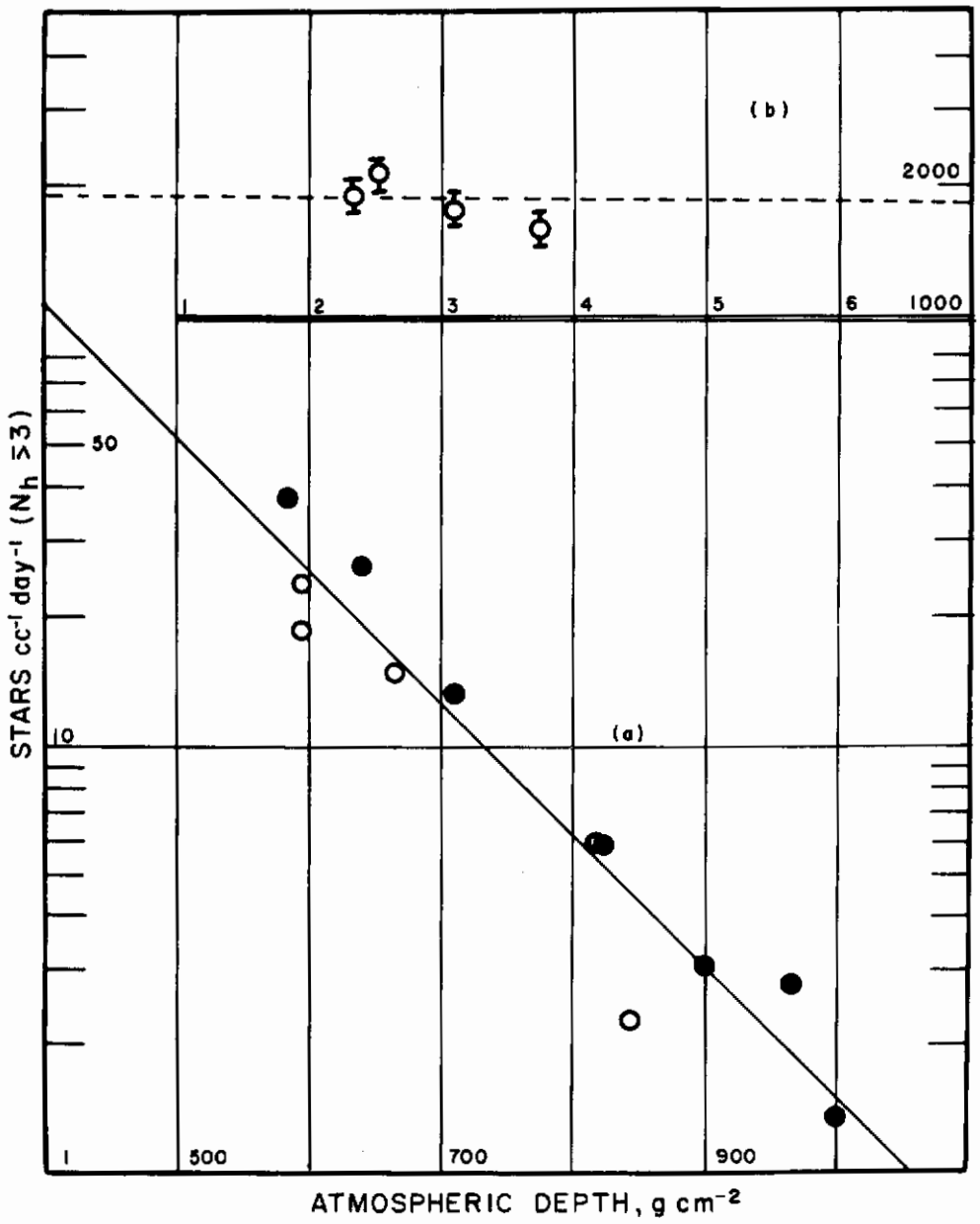

Figure 8. Variation of star production frequency with atmospheric depth.
(a) Within the atmosphere.
(b) Current balloon flight data near top of atmosphere. The dashed line is an extrapolation of curve (a).

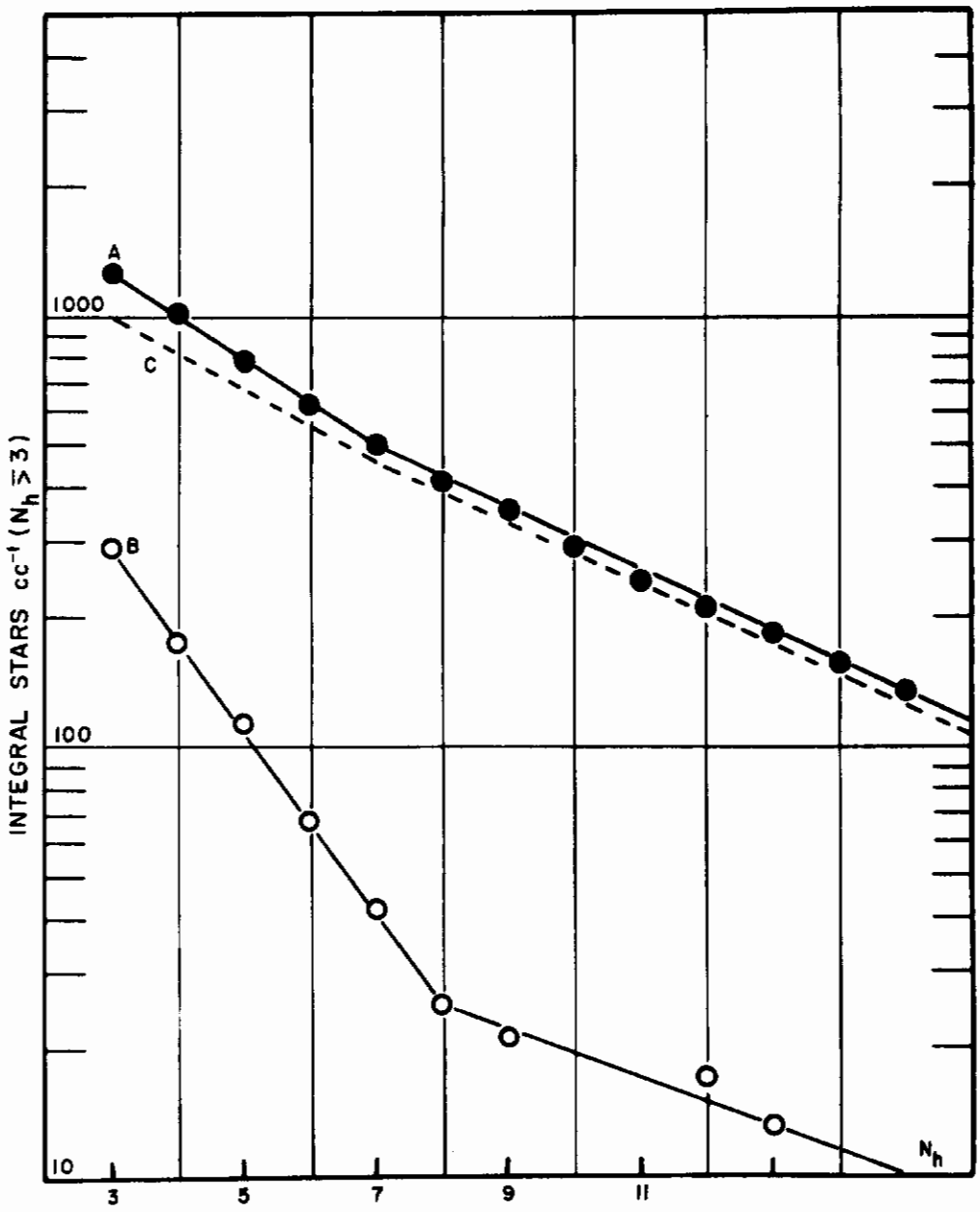

Figure 9. Average star prong spectrum observed on Bemidji balloon exposures A and their accompanying ground controls B. The dashed C indicates the spectrum corrected for background.

sion block in the absence of large masses of condensed matter, the star-size distribution could probably be fitted closely by a single exponential function.

4. Proton-Ender Frequency

In 1959, C.J. Waddington[7] proposed the use of the density of particles which terminate their range in emulsion - "ender-tracks", as a simple parameter for studying temporal variations in the primary cosmic ray flux. In a normal exposure to galactic cosmic radiation the ending tracks largely reflect the production rate of secondary protons and alpha particles produced in nuclear disintegration processes, abetted by a small flux of low energy primaries capable of entering the emulsion detector at the particular air and geomagnetic cutoffs. It differs from a direct star count in that additional ending particles originate from proton recoils and 1-and 2-prong stars, which are not tallied in the conventional nuclear evaporation process. If the emulsion is exposed to an additional flux of low energy solar protons the density of "enders" will increase, whereas the star count would remain essentially unaltered unless the solar flare also produced high energy star producing protons.

Experimentally, a known volume of emulsion is scanned for tracks which terminate their range in the fields of view, basing track selection on the following criteria:

(1) The terminating tracks must have a range ≥ 60 microns, thus excluding all alpha particles originating from radioactive impurities.

(2) Slow electron and meson tracks are excluded.

(3) When the center of a star appears in the field of view, only those tracks are tallied which terminate within the confines of the swath lines with range ≥ 60 microns. Waddington employed an eyepiece reticule defining a square field of 310 microns edge. Our observations were made with smaller

cells of 242 microns edge, in order to cope with the greater density of tracks in our exposures.

(4) If the terminal grain of a track coincided with a field line it was assigned a weight of one half.

The total number of enders per cc Σ has to be corrected for background (A) and tracks accumulated during the ascending and falling phases of the balloon flight (B). Correction (A) could be made from a study of accumulated ender tracks in the control plates. The (B) correction was evaluated with the aid of Waddington's data secured from exposures at different altitudes up to 78,000 ft. His studies indicate that for atmospheric depths less than 30 g cm^{-2} the rate of production of ending particles is independent of altitude, and presumably remains constant to the top of the atmosphere. The differential $\Sigma - \Sigma_{AB}$ can then be expressed as a production rate, ϵ = enders cc^{-1} $hr.^{-1}$ This parameter appears to be an intensive property, independent of the amount of overlying local matter, for normal galactic cosmic ray exposures within or near the top of the atmosphere.

As seen in Table V, the ender production rate was essentially the same on all four of the current balloon flights, the magnitude varying between 498 to 604 enders cc^{-1} $hr.^{-1}$ This parameter is about the same magnitude as that observed by Waddington[8] in balloon flights conducted at geomagnetic latitudes ~55°N (Table VI), which suggests that the Bemidji flights did not encounter a solar flare of appreciable intensity. As a basis of comparison, during the 3+ flare of 12 November 1960, emulsions exposed at 6 g cm^{-2} atmospheric depth by the University of Minnesota Balloon Group exhibited ender intensities of about 10^6 cc^{-1} $hr.^{-1}$

The ender frequencies recorded in Table V were measured in the horizontally oriented animal monitor plates which were exposed under 1.05 g cm^{-2} of condensed matter in addition to the air mass above the balloons. Had appreciable fluxes of solar protons existed with energies $\geq$ 60 Mev, the entering particles would have augmented the ender count. The external package on the flight of 29 July 1960 had a minimum absorber path from the

Table V. Ender Production on Bemidji Balloon Exposures

Flight Date	17 July 60	23 July 60	29 July 60	5 Aug 60
Avg. Plateau, Km	40.0	38.6	42.1	41.5
Total Enders, cc^{-1}	10,029	9,696	10,930	9,610
Background Enders, cc^{-1}	2,969	2,969	2,969	2,969
Total Effective Exposure, Hr *	13.48	13.52	13.18	12.46
ϵ cc^{-1} hr^{-1}	524 ± 36	498 ± 35	604 ± 43	533 ± 37
Stars, cc^{-1} hr^{-1}	74.0	65.9	78.4	88.0
Ratio ϵ/Stars	7.09	7.58	7.71	6.06
Total Absorber, g cm^{-2}	4.15	4.79	3.38	3.58
E_{min} Protons, Mev	66	71	58	60

*The effective exposure incorporates correction B by giving small intervals of flight time a weight proportional to the value of the ender rate at the instantaneous altitude.

Table VI. Ender Frequency on Balloon Flights at Northern Localities (Waddington[8])

Location	Date	g cm^{-2}	cc^{-1} hr^{-1}
Manitoba	3 Aug 58	4.5	580 ± 33
Minnesota	18 Sep 56	6.7	950 ± 50
Minnesota	14 June 58	4.1	435 ± 37
Minnesota	30 July 57		520 ± 40
S. England	9 July 54	10.0	567 ± 33
S. England	20 Nov 58	25.0	432 ± 33
N. England	29 July 59		486 ± 35
N. Missouri	28 Sep 56		670 ± 51

vertical of 2.5 g cm^{-2} . An ender count at 2 mm from the top of the emulsion block, a region accessible to 57 Mev protons, gave an ender count of 555 ± 53 cc^{-1} hr^{-1}. This value is indistinguishable, within statistical variations, from that measured on the animal monitor plate.

The ender frequency and the ratio of enders to stars appear to be potentially useful parameters in making rapid evaluations of exposures to abnormal fluxes of protons, which can originate from solar flares or exposures in the trapped radiation belts. Thus, in emulsions flown into the lower Van Allen belt by an Atlas rocket, the Σ/s ratio was 20 ± 2. Likewise, a high value for this ratio of 22 ± 2 was observed on the Discoverer 18 emulsion block, which reached an apogee of 685 ± 10 km and hence grazed the inner radiation belt. On the other hand, Discoverer 25, whose apogee of 410 km limited the exposure to essentially galactic cosmic radiation, shows a Σ/s = 8.7 ± 1 of the same magnitude as that observed on the current balloon flights.

5. Heavy Primary Thindown Frequency

The heavy primary thindown frequency in emulsion is essentially a special type of ender count for particles of $Z \geq 6$. While this determination is more time consuming than a proton ender count, the additional effort is warranted because of the bioastronautical importance of this category of densely ionizing particles. In addition, it has been shown by a series of studies conducted over a solar sunspot cycle that near the top of the atmosphere the frequency of heavy primary enders varies by a large factor between periods of sunspot maximum and minimum[14].

The conspicuous character of the heavy primary thindowns permits the rapid survey of large volumes of emulsion at 100X magnification. The charge cutoff at $Z \geq 6$ necessitates a quantitative charge of decision for the lighter nuclei $Z = 6 \pm 1$. This identification is effected by counting delta rays at the position of delta ray maximum, as described in an earlier publication[13]. It is well established that heavy primary thindowns are completely attenuated in the atmosphere at altitudes below 60,000 ft. This elevation has, therefore, been

selected as an origin in evaluating the effective time of exposure for the thindown tracks. A more accurate exposure period can be evaluated by expressing the balloon trajectory in terms of the effective solid angle, $\omega(\lambda, h)$, viewed by the emulsions as a function of time. A numerical integration of the 29 July 1960 balloon trajectory indicates that the more exact exposure time was 11.8 hrs. This would increase the frequencies recorded in Table VII by about 8 percent.

Table VII. Termination Frequency of Heavy Primary Nuclei of $Z \geq 6$ in Bemidji Exposures

Flight Date	17 July 60	23 July 60	29 July 60	5 Aug 60
Avg. Plateau, Km	40.0	38.6	42.1	41.5
Hrs. Above 60,000 ft	13.25	13.38	12.94	12.31
No. of Thindowns	26	19.5	189	68
Volume, cc	5.16	5.31	46.69	16.70
Population, cc^{-1}	5.02	3.67	4.04	4.07
Frequency, cc^{-1} day^{-1}	9.1 ± 1.8	6.6 ± 1.5	7.5 ± 0.6	7.9 ± 1.0
Daily Sunspot No.	131	127	94	25

No significant variations were observed in the thindown frequency over the period of 17 July to 5 August 1960. The last flight occurred on a day of exceptionally low sunspot activity, comparable to that of solar sunspot minimum. If the flux of radiation had altered immediately with magnetic field changes associated with the sunspots, our 1953 measurements would have indicated 27 thindowns cc^{-1} day^{-1} for the particular balloon elevation. The value of 7.9 ± 1.0 observed does not differ significantly from the other three flights on which the sunspot activity was normal for the monthly period. It would thus appear that the long range inverse correlation between cosmic ray and sunspot activity over an eleven-year cycle does not apply to daily variations in the cycle. Similar conclusions have been drawn by Neher[2] from measurements of total ionization near the top of the atmosphere on days when the sunspot activity deviated markedly from the seasonal value.

For an average elevation of 140,000 ft, extrapolation of our earlier measurements would indicate 4.7 thindowns cc^{-1} day^{-1} at sunspot maximum. Since the peak of sunspot activity was three years past, the appreciably higher values observed during July of 1960 are consistent with the variations of this parameter within the solar cycle.

References

1. Birnbaum, M., M.M. Shapiro, B. Stiller and F.W. O'Dell, "Shape of cosmic ray star-size distributions in nuclear emulsions", Phys. Rev. 86: 86-89, (1952).

2. Neher, H.V., Proc. Inter. Conf. on Cosmic Rays and the Earth Storm, Sep 1961, Kyoto, Japan.

3. Ney, E.P., J.R. Winckler, and P.S. Freier, "Protons from the Sun on May 12, 1959," Phys. Rev. Letters, 3: 183-185, (1959).

4. Ney, E.P. and W. Stein, Amer. Geophys. Union Abst., Washington, Apr 1961, p.26.

5. Page, N., "Some observations on the nuclear disintegrations caused by cosmic rays in photographic emulsions", Proc. Phys. Soc. (London), A 63: 250, (1950).

6. Teucher, M., "Sterne in Photographischen Platten", Kosmische Strahlung, edited by W. Heisenberg, Berlin, 1953, pp. 69-95.

7. Waddington, C.J., "The study of cosmic ray variations with nuclear emulsions", Nuovo Cimento, 14: No. 6, 1205-1215, (1959).

8. Waddington, C.J., "Note on ending particles in nuclear emulsions exposed to the primary cosmic radiation", Nuovo Cimento, 18: 820-822, (1960).

9. Winckler, J.R., Proc. Conf., "Radiation Problems in Manned Space Flight," NASA, 21 June 1960, Appendix A, pp. 72-93.

10. Winckler, J.R., "Primary Cosmic Rays", Radiation Res. 14: 521-539, (1961).

11. Yagoda, H., unpublished method.

12. Yagoda, H., Unpublished observations of star production in G5 emulsion exposed at Denver, Colorado (1.5 km), Mt. Washington (1.6 km), Climax, Colorado (3.5 km), Mt. Evans and Mt. Rainier (4.3 km), during 1949-50.

References (Cont)

13. Yagoda, H., "Frequency of Thindown Hits by Heavy Primary Nuclei in Emulsion and Tissue", J. Aviation Med. 27: pp. 522-532, (1956).

14. Yagoda, H., "Cosmic Ray monitoring of the manned Stratolab balloon flights", Geophysics Res. Note No. 43, AFCRL-TN-60-640, Sep 1960.

GRD RESEARCH NOTES

No. 1. Contributions to Stratospheric Meteorology, *edited by George Ohring, Aug 1958.*

No. 2. A Bibliography of the Electrically Exploded Wire Phenomenon, *W. G. Chace, Nov 1958.*

No. 3. Venting of Hot Gases Through Temperature Inversions, *M. A. Estoque, Dec 1958.*

No. 4. Some Characteristics of Turbulence at High Altitudes, *M. A. Estoque, Dec 1958.*

No. 5. The Temperature of an Object Above the Earth's Atmosphere, *Marden H. Seavey, Mar 1959.*

No. 6. The Rotor Flow in the Lee of Mountains, *Joachim Kuettner, Jan 1959.*

No. 7. The Effect of Sampler Spacing on Basic Analyses of Concentration Data, *Duane A. Haugen, Jan 1959.*

No. 8. Natural Aerosols and Nuclear Debris Studies, Progress Report I, *P. J. Drevinsky, C. E. Junge, I. H. Blifford, Jr., M. I. Kalkstein and E. A. Martell, Sep 1958.*

No. 9. Observations on Nickel-Bearing Cosmic Dust Collected in the Stratosphere, *Herman Yagoda, Mar 1959.*

No. 10. Radioactive Aggregates in the Stratosphere, *Herman Yagoda, Mar 1959.*

No. 11. Comments on the Ephemerides and Constants for a Total Eclipse of the Sun, *R. C. Cameron and E. R. Dyer, May 1959.*

No. 12. Numerical Experiments in Forecasting Air and Soil Temperature Profiles, *D. W. Stevens, Jun 1959.*

No. 13. Some Notes on the Correlation Coefficient, *S.M. Silverman, May 1959.*

No. 14. Proceedings of Military Geodesy Seminar, December 1958, Air Force Cambridge Research Center *(U), edited by O. W. Williams, Apr 1959. (SECRET Report)*

No. 15. Proceedings of the First Annual Arctic Planning Session, November 1958, *edited by Joseph H. Hartshorn, Apr 1959.*

No. 16. Processes for the Production and Removal of Electrons and Negative Ions in Gases, *S.M. Silverman, Jun 1959.*

No. 17. The Approximate Analysis of Zero Lift Trajectories, *Charles Hoult, Aug 1959.*

No. 18. Infrared Measuring Program 1958 (IRMP 58) – Activities, Achievements, and Appraisal *(U), M.R. Nagel, Jul 1959. (SECRET Report)*

No. 19. Artificial Radioactivity from Nuclear Tests up to November 1958, *E. A. Martell, Sep 1959*

No. 20. A Preliminary Report on a Boundary Layer Numerical Experiment, *M.A. Estoque, Oct 1959.*

No. 21. Recent Advances in Contrail Suppression, *(U), S. J. Birstein, Nov 1959. (CONFIDENTIAL Report)*

No. 22. A Note Comparing One Kilometer Vertical Wind Shears Derived from Simultaneous AN/GMD-1A and AN/GMD-2 Winds Aloft Observations, *H. A. Salmela and N. Sissenwine, Oct 1959.*

No. 23. Atmospheric Refraction of Infrared Radiation, *T. P. Condron, Oct 1959.*

No. 24. Natural Aerosols and Nuclear Debris Studies, Progress Report II, *M. I. Kalkstein, P. J. Drevinsky, E. A. Martell, C. W. Chagnon, J. E. Manson, and C. E. Junge, Nov 1959.*

No. 25. Observations of Jupiter Missile Re-Entry, *(U), R. G. Walker, R. E. Ellis and R. E. Hunter, Dec 1959. (SECRET Report)*

No. 26. Space Probes and Persistence of Strong Tropopause Level Winds, *H. Salmela and N. Sissenwine, Dec 1959.*

No. 27. A Relativistic Treatment of Strong Shock Waves in a Classical Gas, *A. W. Guess, Dec 1959.*

No. 28. Measurements of Flux of Small Extraterrestrial Particles, *H. A. Cohen, Jan 1960.*

No. 29. Proceedings of the Second Annual Arctic Planning Session, October 1959, *edited by Vivian C. Bushnell, Dec 1959.*

No. 30. Atmospheric Pressure Pulse Measurements, *(U), Elisabeth F. Iliff, Jan 1960. (SECRET Report -- Formerly Restricted Data)*

GRD RESEARCH NOTES (Continued)

No. 31. A Discussion of the Calder Equation for Diffusion from a Continuous Point Source, *W. P. Elliott, May 1960.*

No. 32. Lagrangian and Eulerian Relationships in the Absence of Both Homogeneity and Time Steadiness, *M. L. Barad and D. A. Haugen, May 1960.*

No. 33. Thermal Radiation from Rocket Exhausts at Extreme Altitudes, *(U) R. G. Walker, R. E. Hunter, and J. T. Neu, Jun 1960. (SECRET Report)*

No. 34. Thermal Radiation Measurement from an Aerobee Hi Research Rocket, *R. G. Walker, and R. E. Hunter, Dec 1960.*

No. 35. Additional Note -- Strong Vertical Wind Profiles and Upper-Level Maximum Wind Speeds Over Vandenberg Air Force Base. *H. A. Salmela and N. Sissenwine, May 1960.*

No. 36. Contributions to Satellite Meteorology, Vol. I., *edited by W. K. Widger, Jr., Jun 1960.* Vol. II., *edited by F. R. Valovcin, Apr 1961.*

No. 37. IRMP Participation in Operation Big Arm -- Activities, Results and Appraisal *(U), Final Report, M. R. Nagel, et al, Jun 1960. (SECRET Report)*

No. 38. Examples of Project Tiros Data and Their Practical Meteorological Use, *W. K. Widger, Jr., July 1960.*

No. 39. Exploration of the Ionosphere with Telemetering Monochromators and Retarding Potential Analyzers, *H. E. Hinteregger, Aug 1960.*

No. 40. Proceedings of the Second Annual AFCRC Seminar on Military Geodesy, *edited by T. E. Wirtanen, (SECRET Report) Nov 1960.*

No. 41. Tangential Velocity Measurements - An Independent Approach to Geodesy, *B. C. Murray and N. H. Dieter, Sep 1960.*

No. 42. Topographic Charts at One-Degree Intersections for the Entire Earth, *L. Berkofsky and E. A. Bertoni, Sep 1960.*

No. 43. Cosmic-Ray Monitoring of the Manned Stratolab Balloon Flights, *Herman Yagoda, Sep 1960.*

No. 44. Methods for the Evaluation of the Green's Function Arising in the Linear Barotropic Numerical Weather Prediction Theory, *L. Berkofsky, Nov 1960.*

No. 45. Observation of Thor Missile Re-entry, *(U) R. Ellis, Oct 1960. (SECRET Report)*

No. 46. Background Measurements During the Infrared Measuring Program 1956 (IRMP 56) (Unclassified excerpts from the proceedings of the symposium on IRMP-56), *edited by Max R. Nagel, Nov 1960.*

No. 47. Wind Speeds from GMD-1 Ascents Computed Electronically Compared to Plotting Board Results, *H. A. Salmela, Oct 1960.*

No. 48. The Numerical Solution of Fredholm Integral Equations of the First Kind, *J. T. Jefferies and F. Q. Orrall, Nov 1960.*

No. 49. Infrared Spectra of High Altitude Missile Plumes, *(U), Lt. R. E. Hunter, Jan 1961. (SECRET Report)*

No. 50. Aids for Computing Stratospheric Moisture, *Murray Gutnick, Jan 1961.*

No. 51. Some Applications of the Method of Least Squares to Estimating the Probability of a Future Event, *I. A. Lund, Jan 1961.*

No. 52. Winds and Circulations in the Mesosphere, *T. J. Keegan, Feb 1961.*

No. 53. Gravity Observations Along the Northern Coast of Ellesmere Island, *F. A. Crowley, Feb 1961.*

No. 54. Radiation Studies from Nuclear Emulsions and Metallic Components Recovered from Polar Satellite Orbits, *H. Yagoda, Mar 1961.*

No. 55. Proceedings of the Third Annual Arctic Planning Session, November 1960, *edited by G. Rigsby and V. Bushnell, April 1961.*

No. 56. Horizontal Sounding Balloon Feasibility Study *Maj. T. Spalding and S. B. Solot, May 1961.*

No. 57. Instability and Vertical Motions in the Jet Stream, *J. P. Kuettner and G. S. McLean, May 1961.*

No. 58. A Study of Sacramento Peak Flares II: Flare Areas and Importance Classifications, *(to be published).*

No. 59. A Study of Sacramento Peak Flares I: Distribution, Areas, and Growth Curves, *H. J. Smith, April 1961.*

No. 60. Hourly Rawinsondes for a Week, *A. Court and E. A. Salmela, July 1961.*

No. 61. New Vacuum Ultraviolet Emission Continua in the Rare Gases, *R. E. Huffman, W. W. Hunt, Y. Tanaka, R. L. Novak, and J. C. Larrabee, July 1961.*

No. 62. Bibliography of Lunar and Planetary Research - 1960 (With Annotations), *J. W. Salisbury and L. T. Salisbury, Jul 1961.*

No. 63. Flight Information and Experimental Results of Inflatable Falling Sphere System for Measuring Upper-Air Density, *G. A. Faucher, R. W. Procunier and C. N. Stark, Aug 61.*

No. 64. Maximum Winds and Missile Responses, *H. A. Salmela and A. Court, Aug 61.*

No. 65. Meteorological Evaluation and Application of Rainfall Radioactivity Data, *Per B. Storebø, Aug 1961.*

No. 66. The Formation of Ions in the Upper Atmosphere, *R. E. Huffman, (to be published).*

No. 67. Studies in Lunar Topography, *Zdenek Kopal, (to be published).*

No. 68. An Example of Chromospheric Striation Obscuration by a Great Flare, *H. J. Smith and W. D. Booton, Aug 61.*

No. 69. A Numerical Method for Computing Radiative Temperature Changes Near the Earth's Surface, *W. P. Elliott and D. W. Stevens, Sep 61.*

No. 70. Location of a Lunar Base, *J. W. Salisbury and C. F. Campen, Jr., (to be published).*

No. 71. Micrometeorite Collection from a Recoverable Sounding Rocket, *R. K. Soberman, et al, (to be published).*

No. 72. Micrometeorite Measurements from the Midas II, (1960 Zeta 1) Satellite, *R. K. Soberman and L. Della Lucca, Nov 61.*